Received: 25 June 2021 | Revised: 17 September 2021 | Accepted: 21 September 2021

DOI: 10.1002/esp.5258

RESEARCH ARTICLE

ESPL WILEY

Characterization of (paleo)lacustrine landforms using sedimentological and portable OSL investigations at Schweriner See, north-eastern Germany

Marie-Luise Adolph | Reinhard Lampe | Sebastian Lorenz | Torsten Haberzettl

Physical Geography Department, Institute for Geography and Geology, University of Greifswald, Greifswald, Germany

Correspondence
Marie-Luise Adolph, Physical Geography Department, Institute for Geography and Geology, University of Greifswald, Friedrich-Ludwig-Jahn-Str. 16, Greifswald 17489, Germany.
Email: marie-luise.adolph@uni-greifswald.de

Funding information
German Research Foundation (DFG), Grant/Award Number: HA5089/14-1; Ministry of Agriculture and the Environment of the Federal State of Mecklenburg-Western Pomerania; University of Greifswald/Federal State Mecklenburg-Western Pomerania: Graduate Scholarship (Landesgraduiertenstipendium)

Abstract

We investigated four subaerial (paleo)lacustrine landforms at the north-eastern shoreline of Schweriner See, north-eastern Germany. These included two beach ridges, one subaerial nearshore bar and a silting up sequence located close to a fossil cliff, which marks the former maximum extent of Schweriner See. We used luminescence profiling with a SUERC portable OSL device (POSL) on all four sediment sequences in combination with sedimentological investigations such as grain size, loss-on-ignition and magnetic susceptibility to provide information on the various formations in a lacustrine depositional environment. The POSL reader was used on pre-treated polymineral samples to gain an insight into luminescence distribution within the individual sediment sequences, but also among the four sequences. POSL proved valuable to understand depositional processes, which were not visible in lithology or sedimentological parameters. With somewhat larger uncertainty this method provides relative chronologies of the sediment sequences. Additionally, we carried out radiocarbon dating and full optical stimulated luminescence (OSL) dating to establish a chronological framework. OSL ages proved to be more reliable to date beach ridges in this setting than radiocarbon samples, which were severely influenced by sediment reworking. This combined approach of sedimentological analyses, luminescence profiling and absolute age determinations revealed details in depositional processes at Schweriner See which otherwise would have remained undetected. Furthermore, it helped to set these subaerial (paleo)lacustrine landforms in a chronological framework.

KEYWORDS
beach ridge, beach ridge stratigraphy, lake-level variations, luminescence profiling, nearshore bar formation, POSL, SAR-OSL dating

1 | INTRODUCTION

Paleoshorelines include various depositional landforms, which can be used as a paleoenvironmental record. Especially beach ridges are a potential geoarchive for environmental reconstructions worldwide. They form as depositional landforms at shorelines with shallow shoreface and a minimum amount of accommodation space. Beach ridge development depends on sufficient sediment supply and a strong enough wave energy to deposit predominantly sandy sediment, which results in shoreline progradation (Scheffers et al., 2012; Tamura, 2012). However, beach ridge growth is not only influenced by wave energy and sediment supply, but also by water-level changes, which cause sediment dislocation.

Various definitions have been established (e.g. Bendixen et al., 2013; Goslin & Clemmensen, 2017; Hesp et al., 2005; Otvos, 2000). The term 'beach ridge' is still not precisely defined in coastal sciences (Scheffers et al., 2012), and diverse depositional mechanisms exist for different locations under different conditions

(Storms & Kroonenberg, 2007). Detailed modes of beach ridge development and an extensive overview of localities with beach ridge formation were addressed in several synthesis papers (e.g. Goslin & Clemmensen, 2017; Otvos, 2000; Scheffers et al., 2012; Tamura, 2012). However, the term 'beach ridge' only refers to relict features (Otvos, 2000).

In the past, research on beach ridges has been carried out more frequently in coastal marine settings. However, under favourable conditions beach ridges are also deposited at lake shorelines. Detailed investigations on beach ridges in lake systems have mostly been carried out in large systems such as the Great Lakes, USA (Baedke et al., 2004; Carter, 1986; Fraser & Hester, 1977; Johnston et al., 2007; Petty et al., 1996; Thompson, 1992; Thompson & Baedke, 1995, 1997). However, beach ridge formation is not limited to large lakes. In north-eastern Germany, beach ridges were deposited at shorelines of much smaller lake systems such as Lake Müritz (117 km^2; Küster, 2013; Lampe et al., 2009) or Krakower See (17 km^2; Lorenz, 2007), but also at small Fürstenseer See (2 km^2; Kaiser et al., 2014). Here, we present a set of ridges with different formation mechanisms from the north-eastern shoreline of Schweriner See (Figure 1, 61.54 km^2), which is also located in north-eastern Germany.

To use ridge structures as a paleoenvironmental indicator, a reliable chronology is indispensable (Tamura, 2012). Since beach ridges are mostly composed of siliciclastic material, optically stimulated luminescence (OSL) has proven to be most useful because it can be applied directly to sediment grains to determine burial time (e.g. Dougherty et al., 2019; Preusser et al., 2008; Rhodes, 2011; Tamura, 2012). This method has been widely applied to establish beach ridge chronologies (e.g. Botha et al., 2018; Nott et al., 2009; Preusser et al., 2008; Tamura et al., 2019). In addition to full single-aliquot regenerative OSL (SAR-OSL) dating, the introduction of the SUERC portable OSL reader (Sanderson & Murphy, 2010) proved valuable as a rapid and cost-effective luminescence method to establish relative chronologies and to show inconsistencies in chronologies. The portable OSL (POSL) method enables the interpretation of chronologies and targeted full SAR-OSL sampling (Stone et al., 2019). Previous studies investigated age structures of sediment sequences (Gray et al., 2018; Stone et al., 2015), soil mixing (Stang et al., 2012) or sedimentological processes (Muñoz-Salinas et al., 2012). However, the luminescence signal obtained with the POSL reader is not only a function of post-depositional age, but also of luminescence sensitivity, dose rates and signal resetting (Sanderson & Murphy, 2010). Therefore, parameters such as moisture, organic matter content, mineralogy and the geological background have to be considered for the interpretation (Muñoz-Salinas et al., 2011). An extensive overview and state of the science is given by Munyikwa et al. (2021).

In this study we explore the potential of a combined approach of luminescence profiling with sedimentological analyses to characterize internal sedimentary structures of (paleo)lacustrine landforms found at the north-eastern shoreline of Schweriner See. We investigated

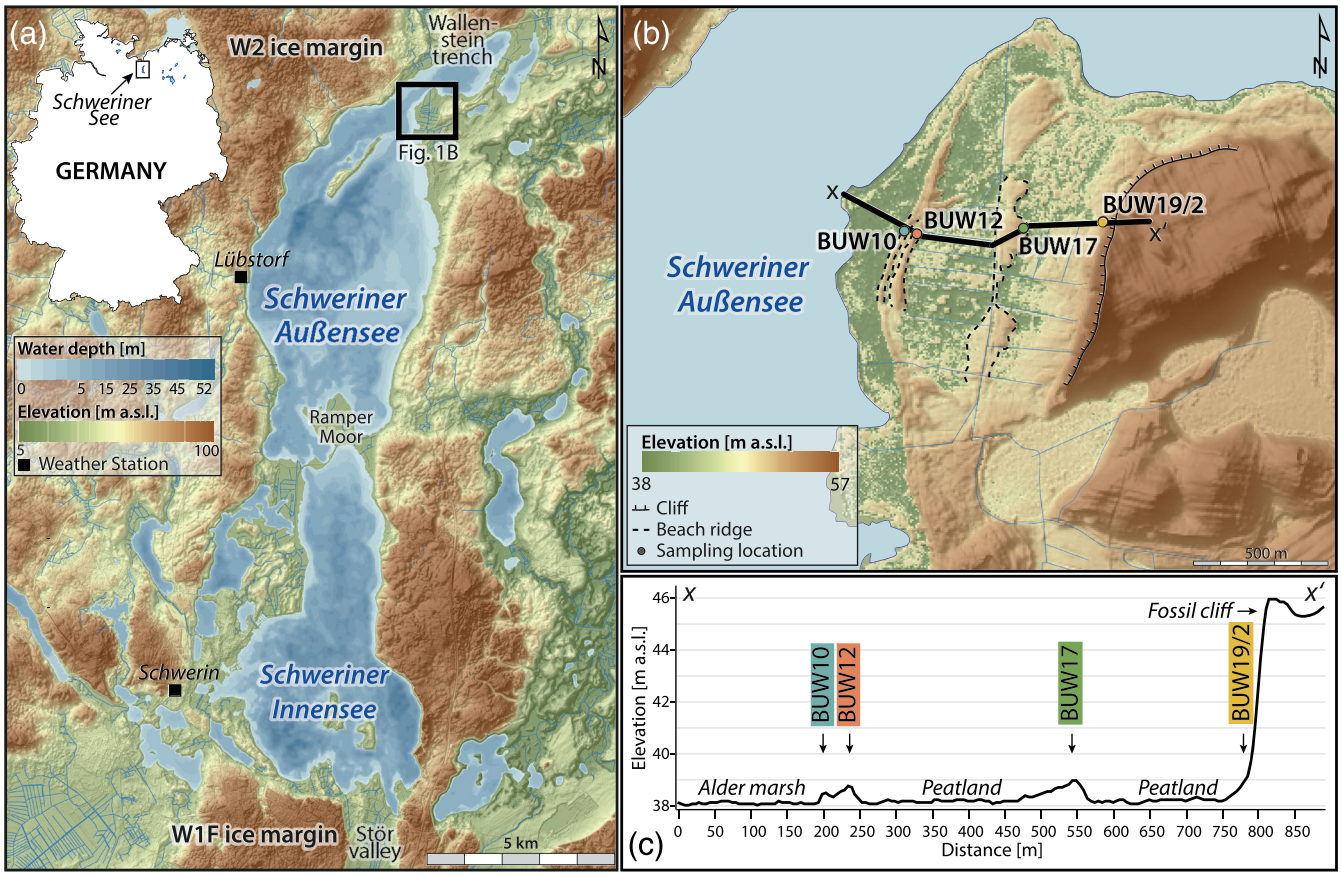

FIGURE 1 (a) Location of Schweriner See in north-eastern Germany (inset) and overview of Schweriner See and surrounding lakes using a digital terrain model in 5 m resolution including water depth. The area of investigation is shown in a bold rectangle. (b) The investigation area 'Buerwischen' is located at the north-eastern part of Schweriner See (square in a). Geomorphological features at the sampling location were investigated using sediment cores as well as soil pits (coloured dots). Dashed lines highlight the width of the ridges. (c) Transect x–x′ shows the elevation of the investigated subaerial ridges extracted from the DEM as well as locations of cores and pits [Color figure can be viewed at wileyonlinelibrary.com]

two beach ridges, one subaerial nearshore bar and one silting-up sediment sequence in front of a fossil cliff which marks the former maximum lake extent. Geochronological data from radiocarbon and full SAR-OSL dating will furthermore support the interpretation and form a chronological framework.

2 | SITE DESCRIPTION

Schweriner See (53°43.256′N, 11°27.544′E, Figure 1) is located at ~37.8 m a.s.l. in the western part of the Mecklenburg lake district (Mecklenburgische Seenplatte), north-eastern Germany, approximately 20 km south of the Baltic Sea. The lake has a surface area of 61.54 km^2 and extends over 24.8 km in the N–S and up to 6 km in the E–W direction. The term 'Schweriner See' refers to two subbasins, which are separated by an (in parts) artificial dam that was completed through a swampy surface (Ramper Moor, Figure 1) to connect the western and eastern shoreline in AD 1848. The northern part is called Schweriner Außensee while the southern basin is named Schweriner Innensee. Today, water exchange between both basins is ensured by a natural channel. The lake has a complex morphometry with several deep areas and channel structures. Schweriner Außensee also has an extended shallow-water area in front of the eastern shoreline, with water depth < 5 m (Figure 1). The shoreline of Schweriner Außensee is mostly surrounded by cliffs of fluvioglacial sediment and only a few accumulation areas, where fossil shore landforms such as beach ridges have been developed and preserved.

Schweriner See is situated between two ice-marginal positions (IMPs) of the Weichselian glaciation: the Frankfurt/Brandenburg IMP in the South and the Pomeranian IMP in the North (Figure 1). The Frankfurt/Brandenburg IMP was dated to 19–18 kyr (Heine et al., 2009) and for the Pomeranian IMP an average age of 16 kyr (Heine et al., 2009; Rinterknecht et al., 2014) was calculated. These ages were dated using cosmogenic ^{10}Be dating and were later recalibrated to 24–21 and 20–25 ka with an updated global ^{10}Be production dataset (Hardt & Böse, 2016). The Frankfurt advance formed the lake basin as a tunnel valley, which was later used as a meltwater channel by the melting Pomeranian advance (Krienke & Obst, 2011). These meltwaters cut through the Frankfurt IMP and created the Stör Valley at the southern end of Schweriner See, which today is the natural outlet of the lake (Figure 1). Outwash sediments from different ice advances are characteristic for the area south of Schweriner See, as well as for the area between the Pomeranian IMP and the lake basin. In between, mainly glaciofluvial sediments, which form plateaus, and ground moraine sediments were deposited and few peatlands emerged (e.g. between both lake basins or at the north-eastern end of Schweriner See) (Krienke & Obst, 2011). The northern outlet, the so-called Wallensteingraben, was built during the 16th century AD through the Pomeranian IMP to connect Schweriner See with the Baltic Sea. The additional drainage most likely led to a lake-level lowering, which has not been quantified until today (von Carmer, 2006). Nowadays, Schweriner See is mainly fed by groundwater, precipitation and surrounding waters, which act as tributaries (Nixdorf et al., 2004).

The recent climate of the study area is documented by the Deutscher Wetterdienst (DWD, German Meteorological Institute). The research area has a mean annual temperature of 9.5°C with the coldest month being January (1.2°C) and the warmest July (18.4°C) (1991–2020, weather station Schwerin; DWD Climate Data Centre, 2021a). Mean annual precipitation is 645 mm with dominating summer rainfalls (1991–2020, weather station Lübstorf; DWD Climate Data Centre, 2021b). However, 2018 was exceptionally dry (442 mm) and warm (10.6°C), which led to a significant drop in lake level, exceeding the minimum operating level. The main wind direction is SSW (194°C, 1964–2019, weather station Schwerin; DWD Climate Data Centre, 2019), which results in a fetch of approximately 8 km for the study area 'Buerwischen' (BUW, Figure 1b). The study area comprises a succession of three subaerial ridge structures (Figures 1b and c) and one silting-up sediment sequence overlain by colluvial layers. The term BUW plus a number (10, 12, 17, 19/2) will be used in the following to distinguish between the different profiles. Profiles BUW10 and BUW12 represent the ridges closest to the recent shoreline. Profile BUW17 is located amidst the plain, while profile BUW19/2 marks the maximum extension of Schweriner See as it is located directly in front of a N–S-oriented fossil cliff (Figure 1). It is up to 750 m from the recent shoreline and reaches a maximum altitude of 39.2 m a.s.l., which is 1.4 m above the modern lake level.

The ridge structures (BUW10, BUW12 and BUW17) are up to 600 m long and 60 m wide. Resulting from the topography, there developed a succession of dry-site vegetation on top of the ridges and wet-site vegetation in a peatland between (Figure 1c). Near the lakeshore, the vegetation is characterized by a peatland dominated by alder. The plain, on which the (paleo)lacustrine landforms developed, extends underwater into a widespread sandy shallow area in front of the recent shoreline.

3 | MATERIALS AND METHODS

Subaerial ridge structures were identified using a DEM5 with a 5 × 5 m resolution before fieldwork (Figure 1b). Positions were recorded with a handheld GPS. Altitudes were determined using the DEM5. Numbers refer to profiles and sediment cores at the same time. Identified key positions of (paleo)lacustrine landforms (BUW10, BUW12, BUW17, and BUW19/2) were studied in-depth. All positions were investigated using soil pits and sediment cores. Photographs, detailed lithological descriptions (grain size, colour, moisture content, percentage of organic matter, carbonate content) following Ad-hoc-AG Boden (2005) and sediment samples for OSL were obtained from the pits. Samples for full SAR-OSL dating and dose rate determination were sampled from each lithological unit in opaque tubes. Additional samples for radiocarbon dating were taken from organic-rich layers (e.g. peat or paleosols) to provide an independent age control. Sediment cores were taken in opaque plastic liners 1 m behind the pit. They were investigated with sedimentological methods and luminescence profiling in the Physical Geography Laboratory of the University of Greifswald. The approach is shown in Figure S1.

Before subsampling, magnetic susceptibility was measured on all sediment cores (Bartington MS2C sensor, diameter 80 mm). Subsequently, all sediment cores were opened under red-light conditions. We pursued luminescence profiling and sedimentological methods (water content and dry bulk density determination, loss on ignition [LOI] as estimate for the organic matter content [OM] and grain size analysis). For luminescence profiling a pre-treatment protocol (carbonate and organic matter removal, dispersing) similar to

the sample preparation for full OSL was applied to reduce the scatter between the samples and to concentrate the targeted quartz and feldspar grains (Gray et al., 2018). The methods are shown in detail in the online Supporting Information Table S1 and Table S2.

For the luminescence profiling we used a POSL reader by the Scottish Universities Environmental Research Centre (SUERC; Munyikwa et al., 2021; Sanderson & Murphy, 2010). All measurements were performed on dried pre-treated polymineral samples, from which approximately 1–2 g was filled in a 3 cm-diameter aluminium cup. The sample surface in the cups was compressed with a light weight to smooth the surface, ensuring a monolayer as well as a consistent distance to the photomultiplier. Each sample was measured twice using fresh unexposed grains each time. The results of both measurements were averaged. In the case of sediment core BUW12, we merged some neighbouring samples (even though it enlarged the sampling distance), because sample quantities were too small to perform reliable measurements.

Infrared (IR) stimulation targets luminescence signals dominated by feldspar. However, Bateman et al. (2015) showed that full depletion is not attained after 60 s IR stimulation due to the limited power of the POSL device and a larger number of grains used in contrast to standard OSL aliquots. Accordingly, the blue-light stimulation (post-IRSL OSL) signal includes a (small) share of IRSL derived by the feldspar signal and cannot be interpreted as pure quartz signal. Nevertheless, an IRSL/OSL ratio was calculated as an approximation to a feldspar/quartz ratio. IRSL and post-IRSL OSL signals were background corrected and depletion indices were calculated. Besides the rapidity of bleaching, the depletion indices of POSL measurements can shed light on grain coatings, with a cleaner grain surface having higher depletion indices if the rest of the parameters are identical (Stone et al., 2019). For the pre-treatment protocol used, the measurement protocol and all calculations, see Table S2 in the online Supporting Information.

Additionally, nine samples were selected for full OSL dating following the standard single-aliquot regenerative (SAR) protocol (Murray & Wintle, 2000, 2003) using a Risø TL/OSL-DA-20 on quartz grains (Table 1). Detailed sample preparation and OSL measurement protocols are shown in Table S3 in the online Supporting Information. Radionuclide contents (K, Th, U) for dose rate calculations were measured with low-level gamma spectrometry (subsamples of ~100 g) at VKTA Rossendorf e.V. (Dresden). The environmental dose rate is crucially affected by the water content in the sediment, presenting a major uncertainty (Preusser et al., 2008). The measured water content is influenced by many factors such as weather, season, vegetation, lake-level changes and artificial drainage canals, which have existed in the investigation area at least since the 1780s. In addition to the site-specific aspects, a change of climate to wetter or drier periods over time must be considered. To reduce the susceptibility to such factors and the influence of measurement errors, the water content for the samples was modelled based on depth, estimated lake-level fluctuations over time, the assumed drainage through the artificial canals and the resulting groundwater level at the sites (Lampe & Lampe, 2018). From this model a time-weighted average for the water content was determined. Additionally, we performed a linear regression as described by Stone et al. (2015) using SigmaPlot 14 to check if ages can be derived from the POSL signals. For this we used the POSL signals from the same depth as the OSL samples. We used the D_e value instead of the already calculated OSL ages and plotted it against the post-IRSL OSL counts (Figure 5a).

AMS-^{14}C dating was carried out as independent age control on 10 samples (Table 2) at the Poznan Radiocarbon Laboratory, Poland. The dating material consisted of wood ($n = 5$), bulk soil samples ($n = 2$), charcoal ($n = 2$), a water plant seed ($n = 1$) and a modern water plant ($n = 1$). Calibration was carried out using Calib 8.20 (Stuiver et al., 2020) with the IntCal20 calibration dataset (Reimer et al., 2020). To differentiate between radiocarbon and OSL dating in the text and figures, they are indicated by a different notation (e.g. calibrated ^{14}C age $= 720\ ^{+145}/_{-40}$ cal BP; OSL age $= 450 \pm 45$ a). As radiocarbon ages correspond to the year AD 1950 and OSL ages to the sampling date, which in this case is AD 2019, there is an offset of 69 years between radiocarbon and OSL ages. This offset cannot be neglected in this study because of the very young ages. To ensure comparability between both dating methods, OSL ages were adjusted to radiocarbon ages by subtracting 70 years, equalling cal BP and a. From here on only adjusted ages will be used. Original and recalculated ages are both shown in Table 1.

4 | RESULTS AND INTERPRETATION

4.1 | Subaerial ridge stratigraphy and relief

The four investigated sedimentary sequences can be subdivided into three depositional types according to their morphology and stratigraphies. The two ridges closest to the lake are represented by profiles BUW10 (38.4 m a.s.l.) and BUW12 (38.8 m a.sl.). Both profiles show similar depositional structures (Figure 2). The sand sequences were deposited on gyttja and peat, indicating former lake and wet-site conditions before ridge deposition. The transition from organogenic sediment to sand is characterized by reworked peat mixed with sand and molluscs (Figure 2). The sand bodies consist of 90 and 80 cm coarse sand. They are stratified sub-horizontally and contain intercalated paleosols. The upper 20–30 cm represents the most recent soil formation. The narrow swale between the two ridges is filled with peat. The width of the individual ridge structures ranges from 20 to 25 m at the examined locations. However, the ridge structure with profile BUW12 broadens to the south up to 50 m. As these two ridges are the nearest to the recent shoreline, they are expected to be the youngest. Sediment sequence BUW17 (39.0 m a.s.l.) is also deposited on calcareous gyttja and peat, which is highly compacted and composed of reed and sedges. In contrast to the other two profiles, the sand body is composed of 170 cm coarse-grained sand, which is rather homogenous. The sediment inclines in the northern direction as evidenced by thin intercalated dipping gravel layers (Figure 2). This might hint at a predominant wave direction from south to southwest, which agrees with the main wind direction measured today. The upper 45 cm represent the recent soil horizon with ploughing marks. The landform with BUW17 is located amidst the plain, approximately 400 m away from the recent shoreline, and is up to 80 m wide. This ridge structure is divided by an approximately 115 m long gap south of the investigated location that continues with a widening ridge (Figure 1b). The ridge with BUW17 is much wider than the first two ridges structures and has a rather slight ascent and a steeper descent in the W–E direction

TABLE 1 Dose rate: paleodose D_e values for the sediment samples from 'Buerwischen'

Lab. No.	Altitude (m a.s.l.)	Below surface (m)	Aliquots (accepted/ measured)	Paleodose D_e (Gy)	OD (%)	U (ppm)	Th (ppm)	K (%)	WC (%)	Cosmic dose (mGy year^{-1})	Dose rate (mGy year^{-1})	Age (a)	Adjusted to ^{14}C* (a)
BUW10													
UG-148	37.94	0.46	26/70	0.42 ± 0.03	27 ± 5	0.37 ± 0.13	1.07 ± 0.09	1.10 ± 0.11	15 ± 4	0.23 ± 0.02	1.27 ± 0.11	330 ± 40	260 ± 40
UG-149	37.80	0.60	15/22	0.68 ± 0.02	10 ± 4	0.35 ± 0.12	0.99 ± 0.08	0.93 ± 0.08	17 ± 4	0.22 ± 0.02	1.1 ± 0.08	630 ± 50	560 ± 50
UG-151	37.55	0.85	16/25	0.51 ± 0.04	28 ± 7	0.33 ± 0.08	0.92 ± 0.08	0.59 ± 0.06	21 ± 4	0.2 ± 0.02	0.77 ± 0.06	660 ± 70	590 ± 70
BUW12													
UG-153	38.25	0.55	32/42	0.67 ± 0.03	24 ± 4	0.54 ± 0.12	1.52 ± 0.12	1.34 ± 0.14	7 ± 4	0.22 ± 0.02	1.64 ± 0.15	410 ± 40	340 ± 40
UG-154	37.85	0.95	56/74	0.63 ± 0.02	21 ± 3	0.69 ± 0.14	1.80 ± 0.14	1.48 ± 0.15	17 ± 4	0.19 ± 0.02	1.63 ± 0.14	390 ± 40	320 ± 40
BUW17													
UG-156	38.10	0.90	18/18	3.60 ± 0.11	11 ± 3	0.37 ± 0.09	1.11 ± 0.09	0.95 ± 0.06	12 ± 5	0.2 ± 0.02	1.15 ± 0.08	3120 ± 230	3050 ± 230
UG-158	37.50	1.50	18/18	4.31 ± 0.21	20 ± 4	0.47 ± 0.09	1.34 ± 0.11	1.28 ± 0.08	16 ± 5	0.18 ± 0.02	1.4 ± 0.09	3080 ± 250	3010 ± 250
BUW19/2													
UG-157	38.30	0.90	22/22	6.95 ± 0.17	10 ± 2	0.61 ± 0.13	1.87 ± 0.14	1.17 ± 0.12	11 ± 5	0.2 ± 0.02	1.45 ± 0.13	4730 ± 450	4660 ± 450
UG-159	38.00	1.20	20/20	13.55 ± 0.48	15 ± 3	0.79 ± 0.19	2.08 ± 0.16	1.13 ± 0.07	12 ± 5	0.18 ± 0.02	1.41 ± 0.1	9530 ± 740	9460 ± 740

Note: All samples were measured on the grain size fraction 200–250 μm. OD – Overdispersion, WC – Water content; *due to a very young age of four samples, all OSL ages were adjusted to radiocarbon ages by subtracting 70 years to ensure better comparability.

TABLE 2 Results of radiocarbon dating

Sample name	Altitude (m a.s.l.)	Material	Lab. No.	Conventional ^{14}C age (BP)	Calibrated ^{14}C age (cal BP)		
					Median	+2σ	−2σ
BUW10 BG 32–34 cm	38.07	Soil	Poz-123669	540 ± 30	550	85	30
BUW10 BG 94–96 cm	37.45	Wood	Poz-122717	825 ± 30	720	60	40
BUW12 BG 80–83 cm	37.98	Charcoal	Poz-122578	850 ± 30	750	145	65
BUW12 BG 30–35 cm	38.48	Wood	Poz-122724	1730 ± 30	1620	80	75
BUW12 BG 155–160 cm	37.23	Wood	Poz-122715	495 ± 30	530	35	25
BUW17 BG 170 cm	37.30	Water plant seed	Poz-123670	4090 ± 35	4600	210	160
BUW17 BG 48 cm	38.52	Soil	Poz-123671	1200 ± 30	1120	120	110
BUW17 BG 160 cm	37.40	Wood	Poz-122579	3950 ± 30	4410	110	120
BUW19/2 57–59 cm	38.62	Charcoal	Poz-122569	1830 ± 30	1730	90	100
BUW19/2 BG 45 cm	38.75	Wood	Poz-122588	560 ± 30	590	50	70
113–20 LPG		Modern water plant	Poz-122570	555 ± 30			

Note: BG refers to samples taken from a pit. If BG in the sample name is missing, sample material is from the sediment core. The dated recent water plant indicates a substantial reservoir effect. All samples were calibrated using Calib 8.20 (Stuiver et al., 2020) and the IntCal20 calibration dataset (Reimer et al., 2020). Samples printed in bold are considered as reliable.

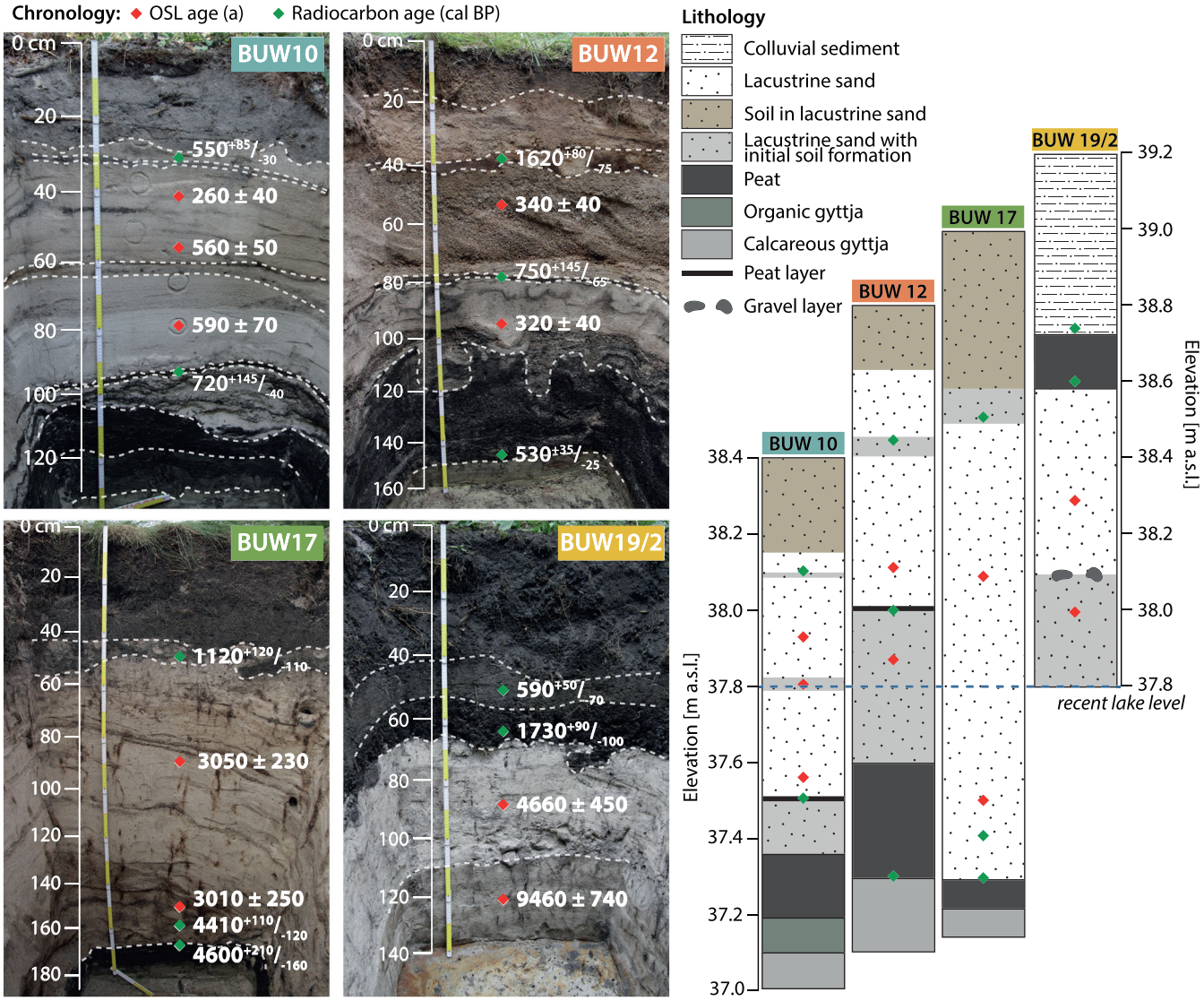

FIGURE 2 Photographs of the investigated pits. Highlighted are radiocarbon (cal BP) and OSL ages (a). OSL ages were recalculated to fit radiocarbon ages by subtracting 70 years to ensure a comparability between both dating methods. Ages printed in bold are considered reliable. Dotted lines represent lithological boundaries used in the simplified lithological sketches, which are shown on the right against altitude (m a.s.l.). The two profiles most proximal to the lake, BUW10 and BUW12, show a multi-layered development. In contrast, profile BUW17 is mostly homogenous with thin intercalated gravel layers. Profile BUW19/2 shows a silting-up sequence close to a fossil cliff representing the maximum extent of Schweriner See. See Figure 1 for the locations of the individual sequences [Color figure can be viewed at wileyonlinelibrary.com]

(Figure 1c). It is up to 39 m a.s.l. high and slopes to 38.1 m a.s.l. both in western and southern directions, where a peatland is formed.

In contrast to the previously discussed ridge structures, profile BUW19/2 (39.2 m a.s.l.) shows an inverse pattern consisting of lacustrine sand deposits overlain by decomposed peat and at least two discernible colluvial layers. Lacustrine deposits are composed of two distinct sand layers intercalated by gravel and stones. The sequence is directly in front of a fossil cliff which represents the former maximum extension of Schweriner See in the eastern direction.

4.2 | Luminescence profiling and sedimentological parameters

Sedimentological parameters (water content, LOI, DBD, mean grain size) and POSL data (IRSL and post-IRSL OSL counts, depletion, IRSL/OSL ratio) allow a subdivision of the four sediment sequences into different units, which in general are consistent with lithological boundaries (Figures 3 and 4). The letter after the sequence name indicates the sedimentological unit and the added roman numbering the subdividing portable OSL unit. Organic-rich lithologies generally form one sedimentological unit, whereas clastic components form a second and in profile BUW19/2 a third one. Clastic units of the sedimentological parameters can further be subdivided into POSL units (Figures 3 and 4).

The three ridge structures BUW10, BUW12, and BUW17 consist of calcareous gyttja as well as peat with an overall small grain size, high organic matter content and a low density forming the lowermost unit A at the bottom. For unit A, no POSL measurements were conducted because the sediment yielded not enough clastic material. Unfortunately, at profile BUW12 the calcareous gyttja at the bottom (Figure 2) was not recovered in the sediment core used for the

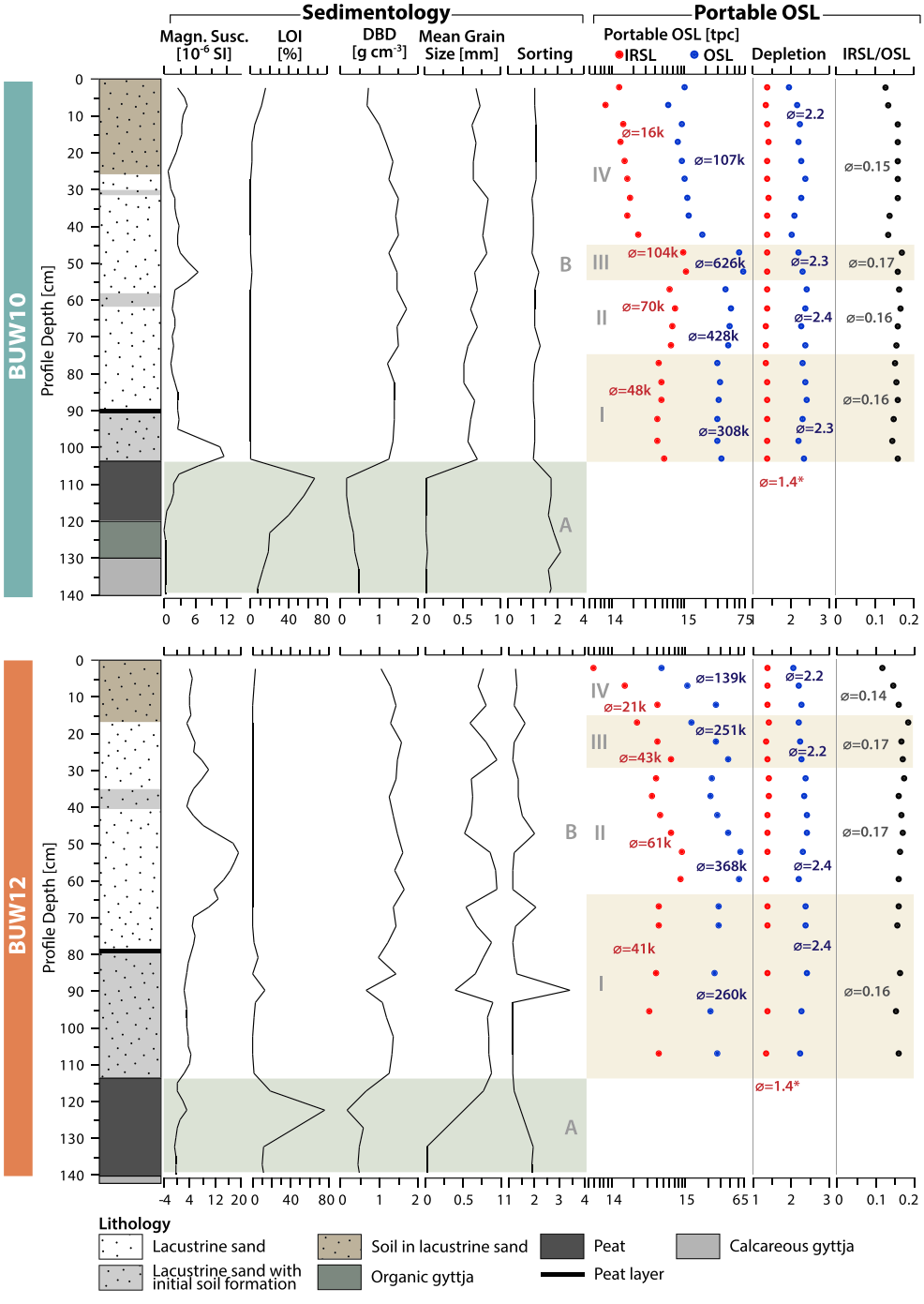

FIGURE 3 POSL and sedimentological data of profiles BUW10 and BUW12. The average POSL data are given for each unit (ø). Average data covering the whole sediment core are marked with an asterisk (*) when the variations were negligible. Sediment cores are characterized in sedimentological units (A and B) and POSL units (given in I–IV, both plotted in grey between sedimentological and OSL data). Note that POSL parameters subdivide sedimentological unit B in both sediment cores [Color figure can be viewed at wileyonlinelibrary.com]

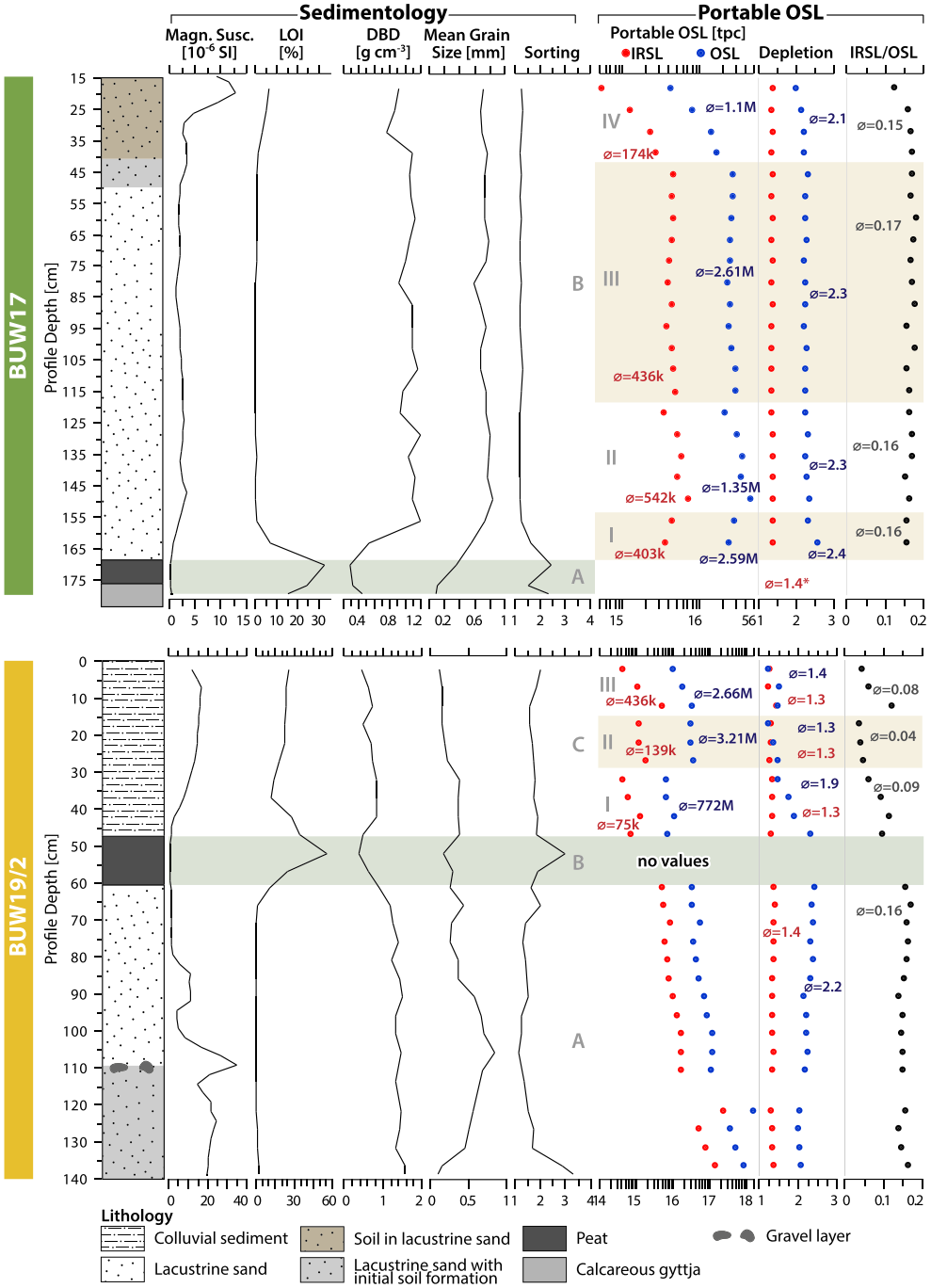

FIGURE 4 POSL and sedimentological data of profiles BUW17 and BUW19/2. The average POSL data are given for each unit (ø). Average data covering the whole sediment core are marked with an asterisk (*) when the variations were negligible. Sediment cores are divided into sedimentological (A–B and A–C) and POSL units (I–III and I–IV), which further subdivide into sedimentological unit B in BUW17 and unit C in BUW19/2. Note that the upper 15 cm in BUW17 are missing [Color figure can be viewed at wileyonlinelibrary.com]

sedimentological analyses (Figure 3). In contrast, unit B consists of sandy sediments in all three ridge structures (BUW10, BUW12, and BUW17). Unit B is characterized by a very low organic matter content, a high density and often coarse sand. Peaks in magnetic susceptibility generally support a beginning soil formation in paleosols (Dearing, 1999), identified in the lithology. In profile BUW12 the highest magnetic susceptibility peak correlates with gravelly coarse sand, which showed hints of iron-coated grains. Unit BUW12-B is much more variable than unit B in BUW10 and BUW17. Here grain sizes and sorting vary. Smaller grain sizes correspond to a poorer sorted sediment. In contrast to the organogenic sedimentation in the other three sediment sequences, unit BUW19/2-A (Figure 5) consists of lacustrine sand at the bottom. It is characterized by low LOI values and a high DBD. Grain size increases towards the centre of the unit, where coarse-grained sediment and a gravel layer are deposited, and decreases again towards the top of the unit. Magnetic susceptibility is high at the intercalated gravel layer. Unit BUW19-B is characterized by a steep increase in LOI, low DBD, small grain sizes and a poor sorting, representing the peat layer already detected in the lithology. In the overlaying colluvial layers in unit BUW19-C, all parameters are on a medium level.

POSL signals subdivide the minerogenic-dominated sedimentological unit B (in BUW19/2 also unit C). BUW10-B is divided into four subunits (Figure 3). Especially noticeable is the reverse structure of both IRSL and post-IRSL OSL values in unit BUW10-B-I, which are lower than units BUW10-B-II and III. This might indicate that units BUW10-B-II and III were poorly bleached before deposition. However, this is not supported by the depletion values. The lower POSL signals in BUW-10-B-I are most likely a result of three different influences. First, this unit has experienced a much higher water content

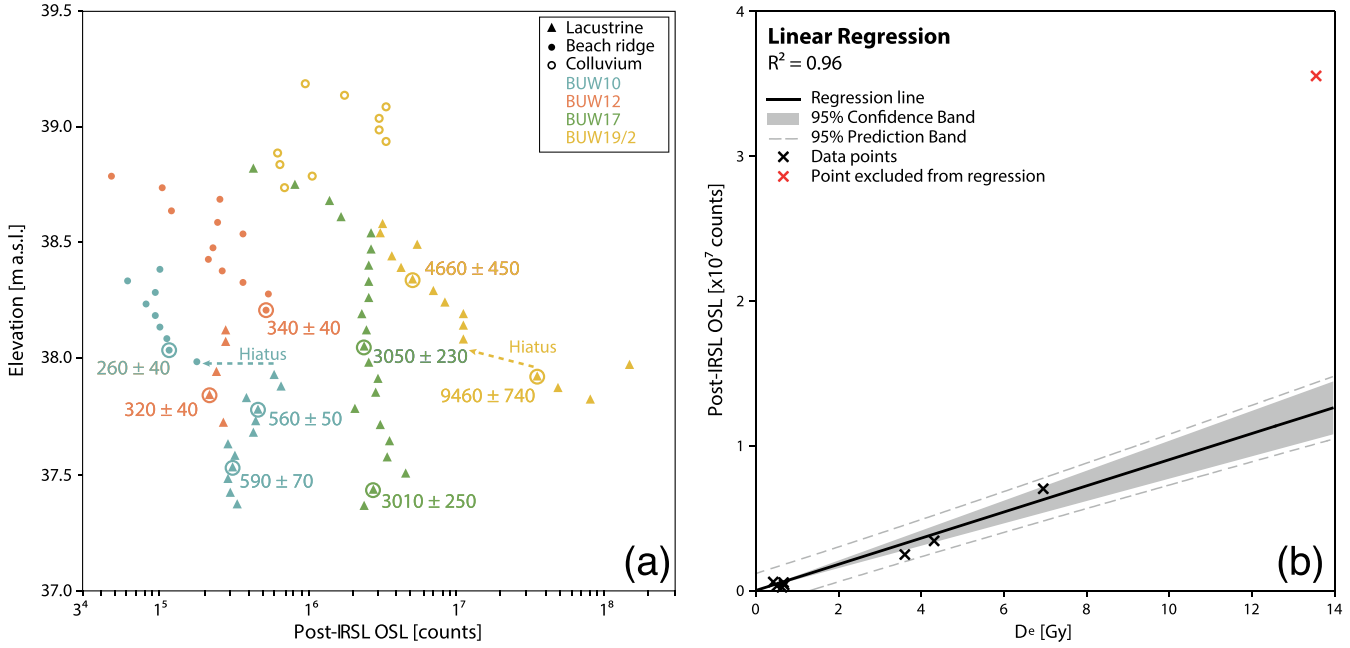

FIGURE 5 (a) Post-IRSL OSL counts are shown against elevation (m a.s.l.). OSL ages are added at their related post-IRSL OSL count and elevation indicated by encircled data points. The profiles have a distinct succession: the further away from the recent shoreline (BUW10 [blue] → BUW19/2 [yellow]) the higher the post-IRSL OSL values are and the older the profiles become. OSL ages were adjusted to radiocarbon ages by subtracting 70 years to ensure comparability between both dating methods. The classification of lacustrine, beach ridge and colluvial sediment is based on sedimentological results. (b) A linear regression between the D_e and post-IRSL OSL values is shown. R^2 is high but the regression is only based on eight data points, out of which five are of a very young age. The oldest data point was excluded due to a different sediment origin [Color figure can be viewed at wileyonlinelibrary.com]

over time, which attenuates the dose rate (Rhodes, 2011). Second, the dose rate itself is much lower in BUW10-B-I than in the overlying unit, with a dose rate of 0.77 ± 0.06 mGy year^{-1} in contrast to 1.1 ± 0.08 mGy year^{-1}. Third, the unit is close to the peat layer underneath, which has an overall lower dose rate. The topmost unit BUW10-B-IV is characterized by a steady decrease in total photon counts towards the top. BUW12-B is highly variable in POSL signals (Figure 3). Starting with almost constant values in BUW12-B-I, IRSL and post-IRSL OSL values are higher at the bottom of unit BUW12-B-II but decrease to the top of the unit. High values at the bottom of this unit might be a result of a higher inherited luminescence in coarse-grained sediment (Bishop et al., 2011). Units BUW12-B-III and IV consist of three samples each, with decreasing values from bottom to top but an offset to higher values at the boundary between both units. The upper two units are furthermore characterized by a slight decrease in depletion. The IRSL/OSL ratio is almost constant in units BUW12-B-I to III but shows a decrease towards the top in BUW12-B-I. In unit BUW17-B-I, both POSL signals show a rising trend which in general is lower than in BUW17-B-II to IV (Figure 4). Total photon counts are almost constant in units BUW17-B-II and III, with slightly more variability in II, which indicates rapid continuous sedimentation. Unit BUW17-B-IV is characterized by a distinct decrease in IRSL and post-IRSL OSL. Depletion and IRSL/OSL ratios are almost constant with minor variations, which indicates both almost consistent bleaching and similar sediment composition.

BUW19/2-A shows a constant decrease in total photon counts to the top, consistent depletion and IRSL/OSL values (Figure 4). The peat layer unit BUW19/2-B did not yield enough clastic material for reliable measurements. Colluvial sediments in unit BUW19/2-C are characterized by highly variable POSL parameters, which allow us to distinguish three different colluvial layers (BUW19/2-C-I to III).

These layers are characterized by distinct offsets in post-IRSL OSL values but also by changes in depletion. However, IRSL depletion remains constant over the entire sequence, whereas post-IRSL OSL drops significantly towards the top, indicating badly bleached sediments. The difference in both parameters might result from the different bleaching times required for quartz and feldspars. Variations in post-IRSL OSL are also mirrored by changes in the IRSL/OSL ratio.

4.3 | Geochronology

The chronological framework (Figure 2) is based on nine OSL ages (Table 1) from the sandy sediment sequences and 10 AMS-^{14}C ages (Table 2) on peat and paleosols. SAR-OSL results were furthermore compared with POSL signals (Figure 5) to get a more detailed insight into the relative age structure of the ridge deposits.

4.3.1 | OSL characteristics

At least 64 % of the measured aliquots per sample (18–70) were accepted according to the quality criteria. An exception is sample UG-148 with only 26/70 accepted aliquots. Paleodoses D_e of the OSL measurements range from 0.42 ± 0.03 Gy (UG-148) to 13.55 ± 0.48 Gy (UG-159) (Table 1). Environmental dose rates vary between 0.77 ± 0.06 mGy a^{-1} (UG-151) and 1.64 ± 0.15 mGy a^{-1} (UG-153). Overdispersion values range between 10 ± 2% (UG-157)

and 28 ± 7 % (UG-151), but in seven out of nine cases are below 25 %. Relative age errors are between 7.42 and 10.92 %, and therefore within a normal range of OSL age uncertainty (Murray & Olley, 2002).

Sample UG-151 marks an overall exception, with a much lower environmental dose rate in comparison to the other samples (Table 1). The much lower potassium value (~0.6 % in contrast to ~0.95–1.48 %, Table 1) points towards a different sediment source. Furthermore, this sample has a high overdispersion and was sampled in proximity to the underlying peat. Peat naturally has a lower dose rate than the surrounding siliciclastic sediment, which has been formed from igneous or metamorphic rocks. We therefore assume that this age is most likely underestimated.

4.3.2 | OSL and radiocarbon ages

For radiocarbon ages in beach ridges, several possible constraints have to be considered. Previously, radiocarbon samples from beach ridges were taken from the swales in between the ridges, which are often filled with peat. However, ages obtained from swales might partially have a large offset to the ridge formation, as ridge and peat did not necessarily form at the same time (Tamura, 2012). For this study, we sampled paleosols and peat layers within the ridge structures for radiocarbon dating. However, sometimes dating material appears to be severely influenced by material dislocation, resulting in unreliable ages. Therefore, we will mostly rely on OSL ages and relative age structures revealed by luminescence profiling. Even though water-lain sediments can be complicated to date (Preusser et al., 2008), they proved to be more reliable than radiocarbon ages.

The most proximal profile to today's lake shoreline, BUW10, was dated to 590 ± 70 a at 37.55 m a.s.l. (UG-151), 560 ± 50 a (UG-149) at 37.80 m a.s.l. and 260 ± 40 a at 37.94 m a.s.l. (Figure 2). Considering the errors, the stratigraphically lower ages are consistent and sediments were deposited almost contemporaneously (i.e. in a geologically very short time period). Considering the distance of only 15 cm between UG-149 and UG-148, either the sedimentation rate decreased significantly or a hiatus occurs between both ages, which is more likely. In contrast, both radiocarbon ages are older. The peat layer at 37.45 m a.s.l. was dated to 720 $^{+145}/_{-40}$ cal BP (Poz-122717) on wood. Although stratigraphically this age is consistent, we suspect this peat layer to be relocated as a peat layer in the same stratigraphic position has a very similar age of 750 $^{+145}/_{-65}$ cal BP in BUW12, which is too old for its stratigraphic position there (Figure 2). In BUW12 this age is above a much younger OSL age, which questions a synsedimentary *in-situ* development of the peat layer and hence the validity of the two radiocarbon ages. It is very likely that the dating material was reworked and depleted radiocarbon was incorporated into the sediment. The topmost paleosol layer in BUW10 at 38.07 m a.s.l. was dated to 550 $^{+85}/_{-30}$ cal BP (Poz-123669) (Figure 2). Considering the very young OSL age below, this indicates incorporation of radiocarbon-depleted organic material, also leading to a too old age estimate for the paleosol layer.

Luminescence dating in profile BUW12 revealed ages of 320 ± 40 a (UG-154) at 37.85 m a.s.l. and 340 ± 40 a (UG-153) at 38.25 m a.s.l. (Figure 2). Although the lower OSL age is younger, both ages are consistent within the error of the method, which—like in BUW10—indicates a very rapid deposition. The three AMS-^{14}C ages are all significantly older and arranged in a reverse chronological order with depth (Figure 2). The only age in stratigraphic order is the youngest age of 530 $^{+35}/_{-25}$ cal BP (Poz-122715) at 37.23 m a.s.l., which was dated on a large piece of wood at the transition from gyttja to a reworked peat layer with molluscs and sand in between. The radiocarbon age of 750 $^{+145}/_{-65}$ cal BP (Poz-122578) at 37.98 m a.s.l. was obtained from charcoal in a thin peat horizon. As discussed for profile BUW10, the age and composition of this peat layer are similar to a peat layer at 37.45 m a.s.l. in profile BUW10, making a contemporaneous reworking of older material likely. The uppermost radiocarbon age of 1620 $^{+80}/_{-75}$ cal BP at 38.48 m a.s.l. (Poz-122724) is based on wood taken from a paleosol, which according to its stratigraphic location is also reworked and depleted in radiocarbon.

The sandy sequence in profile BUW17 was OSL dated to 3010 ± 250 a (UG-158) at 37.50 m a.s.l. and to 3050 ± 230 a (UG-156) at 38.10 m a.s.l. (Figure 2). Considering the error of the dating method as in the two previous ridges BUW10 and BUW12, this indicates a rather rapid deposition. The underlying peat layer formed most likely on-site. The oldest radiocarbon age dates the transition from peat to sand to 4600 $^{+210}/_{-160}$ cal BP (Poz-123670) at 37.30 m a.s.l., which was measured on water plant seeds. As a modern water plant was dated to 555 ± 30 BP, indicating a substantial reservoir effect, this might have affected the age of the water plant seed as well. However, a radiocarbon age of 4410 $^{+110}/_{-120}$ cal BP (Poz-122579) just above the peat layer at 37.40 m a.s.l. carried out on wood (terrestrial origin) supports the assumption that a reservoir effect is negligible in this case. The age offset between this radiocarbon age at 37.40 m a.s.l. and the OSL age at 37.50 m a.s.l. (3010 ± 250 a) of >1500 years within only 10 cm points to a hiatus. The topmost radiocarbon age is dated on bulk sediment and is located at the transition from organic matter-free sand to recent soil formation processes. The age indicates a subsequent landscape stabilization at 1120 $^{+120}/_{-110}$ cal BP (Poz-123671) at 38.52 m a.s.l. The boundary shows indications of ploughing, which could have incorporated younger material. This appears to be very likely, since in all three ridges discussed so far, the deposition in the sandy main part of the ridges occurred very rapidly (also in the lower part of BUW17). If the age of 1120 $^{+120}/_{-110}$ cal BP reflects the time of deposition, the sedimentation rate would have decreased dramatically or sediments would have been eroded. However, due to our luminescences profiles discussed earlier, this is rather unlikely as a rapid continuous sedimentation is suggested.

Profile BUW19/2 was dated by two OSL ages to 9460 ± 740 a (UG-159) at 38.00 m a.s.l. and 4660 ± 450 a (UG-157) at 38.30 m a.s.l. (Figure 2). Samples were taken from two separate lacustrine sand layers, which are intercalated by a coarse gravel layer. It is most likely that a lower lake level occurred between the two OSL ages dated in profile BUW19/2. Very likely this low stand is expressed by a hiatus accompanied by the coarse gravel layer. The decomposed peat overlaying the lacustrine sand is dated to 1730$^{+90}/_{-100}$ cal BP (Poz-122569) at 38.62 m a.s.l., indicating a silting up after a previous maximum extension of Schweriner See reaching (again) to this location. The lowermost colluvial layer above the peat at 38.75 m a.s.l. is dated to 590$^{+50}/_{-70}$ cal BP (Poz-122588, Figure 2).

4.3.3 | POSL and SAR-OSL

We compared the POSL signals from all four profiles (a) to each other regarding their elevation and POSL signal distribution and (b) against the measured OSL ages (Figure 5). The comparison between the different (paleo)lacustrine landforms shows an overall increase in age with increasing distance from the recent shoreline. The youngest two profiles BUW10 and BUW12 show the lowest POSL signals, while BUW19/2's values, which cover the oldest time intervals, are highest (Figure 5a). This was expected, as POSL data are mostly correlated with age even though other factors have to be considered (Muñoz-Salinas et al., 2011). In sediment sequences BUW19/2, a steady decrease in post-IRSL OSL values is in line with a decline in absolute ages. Stable values and ages within each other's error range indicate a rapid sedimentation in profile BUW17. The sharp offset to lower post-IRSL OSL values in BUW10 at 38 m a.s.l., which correlates with a decline in age from 560 $\pm$ 50 to 230 $\pm$ 30 a, indicates a hiatus between both ages. In contrast, the ages of BUW12 with 320 $\pm$ 40 and 340 $\pm$ 40 a fall within the time range of the hiatus in BUW10. This could indicate erosional processes at BUW10 and deposition at BUW12 in the meantime.

Additionally, we compared the D_e against the post-IRSL OSL values using linear regression as proposed by Stone et al. (2015, 2019). The oldest data point (13.55 $\pm$ 0.48 Gy, UG-159) was excluded from the regression as we assume a different sediment source and/or mode of deposition. The material most likely was eroded directly from the cliff, which is composed of glaciolacustrine/fluvial sand. An R^2 of 0.96 indicates a good fit of the model. Despite the scatter, the model implies that in our case the POSL signal seems to correlate mostly with age. But it has to be kept in mind that the regression is only based on eight data points, of which five are of a very young age. Observed scatter in the regression could result from either anomalous fading, differences in luminescence sensitivity, but also from different modes of deposition such as nearshore bar deposition vs. beach ridge deposition, resulting in incomplete bleaching.

5 | DISCUSSION

Luminescence profiling is a useful addition to sedimentological analyses and absolute age determinations like OSL or radiocarbon dating. For the investigation of paleosols and their cover sediments in formerly glaciated areas, Kaiser et al. (2020) remarked that a focus on a larger number of ages for problematic profiles might help to tackle possible constraints. In this study paleosols were unsuitable for radiocarbon dating due to sediment reworking. However, luminescence profiling as a cost- and time-effective method was a tremendous help to disentangle conflicting absolute ages. Luminescence profiling not only offered an indication of relative ages, but also showed changes in sedimentation processes that were not always visible in the sedimentological parameters. This supports the observations by Bateman et al. (2015), who also concluded that luminescence profiling is capable of detecting changes that are not visible in other sediment characteristics. Especially profiles BUW10 and BUW17 showed no clear indication of changes in sedimentation, with almost consistent sedimentological parameters. In profile BUW17, POSL suggests a rapid sedimentation (Figure 4) as nearly no changes occur; results for profile BUW10 revealed a hiatus, which was also confirmed by full SAR-OSL dating (Figure 5). Particularly noticeable is the value of POSL investigations in conjunction with sedimentological analyses in profile BUW19/2-C-III to I (Figure 4). Here three distinct colluvial layers could be identified only with the help of POSL, which not only showed changes in IRSL and post-IRSL OSL values but also in depletion and IRSL/OSL ratio. Considering the lithology and sedimentology only, we would have only detected two colluvial layers.

The luminescence signal in our study seems to be predominantly influenced by an age signal built up after deposition (Figure 5). Similarly, a predominantly age-related POSL signal was previously shown in several studies in various settings (e.g. Bateman et al., 2015; Gray et al., 2018; Stone et al., 2015, 2019). This is also true for the sediment sequences at Schweriner See. The higher the POSL signals are, the older the sediments. The relationship between D_e values and post-IRSL OSL counts is well represented by a linear regression. However, the POSL signal seems to be partially dependent on grain size in the case of profile BUW12, even though we sieved the sediment to <315 μm to reduce the scatter. In profile BUW12, the highest POSL signals correlate with a peak in grain size and magnetic susceptibility. Bishop et al. (2011) also showed a strong correlation between photon counts and grain size, with increasing grain sizes being less bleached and having a higher inherited luminescence in water-lain sediment. The grain size distribution for all profiles from Schweriner See showed predominantly medium and coarse sand with varying percentages. The fine-sand fraction was mostly <5 %, with a few exceptions. However, in BUW12 the grain size composition shifted to almost 96 % coarse grain sand in some samples. Therefore, the composition within the POSL sample also shifted to overall coarser sediment, which might have been less bleached, resulting in higher luminescence values.

In contrast, it is characteristic for profiles BUW10, BUW12 and BUW17 that the POSL signals of the lowest POSL unit (unit B-I in all three profiles) is lower than the POSL signal in the overlaying sediment. This most likely results from the sample location below the recent lake level and from higher lake levels in the past, which is why a different water content for each sample has to be presumed over time. The water content was corrected in the OSL ages, with an adjusted water content for age calculations (Table 1). However, such a correction was not applied to POSL signals. A varying water content over time might also be a reason for the large scatter obtained in the regression analysis (Figure 5). Furthermore, the lowest units are in proximity to the underlying peat, which also attenuates radiation, resulting in lower luminescence signals. We did not measure luminescence on the peat sequences, even though in previous studies POSL was successfully measured on organic-rich untreated sediment samples (Muñoz-Salinas et al., 2011, 2014; Portenga & Bishop, 2016). Here the pre-treatment protocol, according to which carbonates and organic matter were removed, was the limiting factor because the peat yielded not enough clastic material to carry out reliable measurements. Like for full SAR-OSL measurements, this method is bound to clastic material, but a greater sample quantity is required (Bateman et al., 2015).

Particularly prone to changes in luminescence are the two profiles most proximal to today's shoreline. Based on the regression results, age dominates the POSL signal. Therefore, the lower part of profile BUW10 has to be older than profile BUW12, even though profile

BUW10 is located closer to the recent shoreline (Figures 1 and 5) and—logically—should be younger. This age structure is also confirmed by the OSL ages, but raises the question how the deposition of these two ridges occurred, as beach ridge structures usually become younger with proximity to the recent shoreline. Based on the POSL signals, the OSL ages and the sedimentology, the following scenario is assumed: before the two foremost beach ridges were deposited, the lake level was significantly lower, which was shown in archaeological investigations (Konze, 2017). A widespread peat formed, as indicated by the peat layer in BUW10 und BUW12. With a rising lake level, the peat was flooded and lacustrine sand (marked with a triangle in Figure 5) was deposited on top of the peat. Due to an earlier flooding of the lower part of BUW10, which is located closer to the recent shoreline, these ages are older (590 ± 70 and 560 ± 50 a), but do not represent beach ridge formation yet—rather the deposition of lacustrine sand. Therefore, these ages indicate a rising lake level. In profile BUW10 the luminescence profile has an inverse structure for units 10-B-I to 10-B-III, which is most likely the result of a lower dose rate (UG-151 with 0.77 ± 0.06 mGy a^{-1} in contrast to 1.10 ± 0.08 mGy a^{-1} for the overlaying UG-149, Table 1) and not an age-related signal. This might hint at a different sediment source than in all other samples, likely as a result of the lower lake level. Afterwards, with a stabilizing or falling lake level, two beach ridges were deposited on top of the lacustrine sand, resulting in beach ridge formation around 320 ± 40 and 340 ± 40 a for BUW12, as well as 260 ± 40 a for BUW10. This deposition of profile BUW12 most likely represents the time of the hiatus in profile BUW10, which was detected in the POSL signals (transition unit 10-B-III to 10-BIV), as well as in the absolute age determinations (560 ± 50 vs. 260 ± 40 a in 10 cm distance). The overall youngest OSL age of 260 ± 40 a is found in BUW10 and coincides with the construction of the Wallensteingraben. The Wallensteingraben was built to connect the cities of Schwerin and Wismar in the 16th century and in the process a second outflow for Schweriner See was created. This second outflow most likely led to a lowering lake level after final completion (von Carmer, 2006), showing the severe impact human activities had on Schweriner See.

In contrast to these two beach ridge profiles, profile BUW17 suggests a different mode of deposition. We assume that the ridge was deposited as a nearshore bar, which became subaerial by a lowering lake level (Scheffers et al., 2012; Tanner, 1995). The deposition in BUW17 happened rather rapidly as POSL signals, which have almost no variations, suggest.

Modes of beach ridge deposition can differ between sets of beach ridges in the same system (Goslin & Clemmensen, 2017; Nott et al., 2015; Scheffers et al., 2012). At Schweriner See the different stratigraphies point to two modes of deposition. The foremost two ridge structures with profiles BUW10 and BUW12 were deposited during several events, indicated by the intercalated paleosols and organogenic layers. In contrast, profile BUW17 shows no indication of multi-event development, but rather a continuous sedimentation as suggested in the POSL and sedimentological values, which have almost no variations. This hints at either more constant depositional conditions or even a deposition somewhat offshore not directly at the shoreline, which might be more susceptible to changes in grain size due to storm events with varying intensities, wind speeds and directions. Inclining gravel layers suggest a consistent wave direction. A conceivable scenario might be a subaquatic deposition as a nearshore bar, that was exposed by a (rapid?) lake-level decline. The formation of such bars can also be observed today on the shallow water subaquatic extension of the plain. In contrast to the profiles from the ridge structures, profile BUW19/2 represents lacustrine deposits at the former maximum extent of Schweriner See. The lacustrine deposits are covered by peat, which formed after the final lake-level decline and was subsequently buried by colluvial deposits from the adjacent cliff.

6 | CONCLUSION

Luminescence profiling proved very valuable to further subdivide sedimentological units in ridge structures at the north-eastern shoreline of Schweriner See. Furthermore, POSL helped to better understand (paleo)lacustrine landform formation at Schweriner See. We showed that a larger number of time and cost-intensive dating efforts, like OSL ages or radiocarbon ages, are not absolutely necessary—especially if the profiles are highly susceptible to sediment reworking. In this study, radiocarbon ages of paleosols could not be used reliably for the chronology. To overcome these limitations, luminescence profiling using a POSL reader can be employed as a cost- and time-effective method. In this study, luminescence profiles proved invaluable in:

a. identifying additional breaks in sedimentological successions;
b. interpreting sediment structures in greater detail than would have been possible from sedimentological and absolute age data (AMS-^{14}C and OSL dating) alone;
c. understanding beach ridge formation at Schweriner See, where traditional sedimentological parameters showed no indications of depositional change.

Furthermore, this method was especially helpful to understand the origin of conflicting full SAR-OSL ages and to disentangle absolute ages using luminescence profiles based on their relative age structure.

ACKNOWLEDGEMENTS

This research was supported by the Ministry of Agriculture and the Environment of the Federal State of Mecklenburg-Western Pomerania, Germany and the German Research Foundation DFG (HA5089/14-1). MLA received a Graduate Scholarship (Landesgraduiertenstipendium) of the Federal State of Mecklenburg-Western Pomerania/University of Greifswald to conduct this research. Furthermore, we would like to thank Klara Isermann, who supported the field work over two summers, and contributed to fruitful discussions.

DATA AVAILABILITY STATEMENT

The datasets generated and analysed during the current study are available from the corresponding author on reasonable request.

ORCID

Marie-Luise Adolph https://orcid.org/0000-0002-0560-305X
Torsten Haberzettl https://orcid.org/0000-0002-6975-9774

REFERENCES

Baedke, S.J., Thompson, T.A., Johnston, J.W. & Wilcox, D.A. (2004) Reconstructing paleo lake levels from relict shorelines along the Upper Great Lakes. *Aquatic Ecosystem Health & Management*, 7(4), 435–449. https://doi.org/10.1080/14634980490513274

Bateman, M.D., Stein, S., Ashurst, R.A. & Selby, K. (2015) Instant luminescence chronologies? High resolution luminescence profiles using a portable luminescence reader. *Quaternary Geochronology*, 30, 141–146. https://doi.org/10.1016/j.quageo.2014.12.007

Bendixen, M., Clemmensen, L.B. & Kroon, A. (2013) Sandy berm and beach-ridge formation in relation to extreme sea-levels: A Danish example in a micro-tidal environment. *Marine Geology*, 344, 53–64. https://doi.org/10.1016/j.margeo.2013.07.006

Bishop, P., Muñoz-Salinas, E., MacKenzie, A.B., Pulford, I. & McKibbin, J. (2011) The character, volume and implications of sediment impounded in mill dams in Scotland: The case of the Baldernock Mill dam in East Dunbartonshire. *Earth and Environmental Science Transactions of the Royal Society of Edinburgh*, 101(2), 97–110. https://doi.org/10.1017/S1755691010009205

Ad-hoc-AG Boden. (2005) *Bodenkundliche Kartieranleitung KA5*. Schweizerbart: Hannover.

Botha, G.A., Porat, N., Haldorsen, S., Duller, G.A., Taylor, R. & Roberts, H. M. (2018) Beach ridge sets reflect the late Holocene evolution of the St Lucia estuarine lake system, South Africa. *Geomorphology*, 318, 112–127. https://doi.org/10.1016/j.geomorph.2018.06.001

Carter, R.W.G. (1986) The morphodynamics of beach ridge formation: Magilligan, Northern Ireland. *Marine Geology*, 73(3–4), 191–214. https://doi.org/10.1016/0025-3227(86)90015-0

Dearing, J. (1999) *Environmental Magnetic Susceptibility: Using the Bartington MS2 System*. Oakham: Chi Publishing.

Dougherty, A.J., Choi, J.-H., Turney, C.S.M. & Dosseto, A. (2019) Technical note: Optimizing the utility of combined GPR, OSL, and Lidar (GOaL) to extract paleoenvironmental records and decipher shoreline evolution. *Climate of the Past*, 15(1), 389–404. https://doi.org/10.5194/cp-15-389-2019

DWD Climate Data Centre (2019) Hourly mean of station observations of wind direction at ca. 10 m above. Deutscher Wetterdienst: München.

DWD Climate Data Center (2021a) Monthly mean of station observations of air temperature at 2 m above. Deutscher Wetterdienst: München.

DWD Climate Data Center (2021b) Monthly station observations of precipitation in mm for Germany. Deutscher Wetterdienst: München.

Fraser, G.S. & Hester, N.C. (1977) Sediments and sedimentary structures of a beach-ridge complex, southwestern shore of Lake Michigan. *Journal of Sedimentary Petrology*, 47(3), 1187–1200. https://doi.org/10.1306/212F7306-2B24-11D7-8648000102C1865D

Goslin, J. & Clemmensen, L.B. (2017) Proxy records of Holocene storm events in coastal barrier systems: Storm-wave induced markers. *Quaternary Science Reviews*, 174, 80–119. https://doi.org/10.1016/j.quascirev.2017.08.026

Gray, H.J., Mahan, S.A., Springer, K.B. & Pigati, J.S. (2018) Examining the relationship between portable luminescence reader measurements and depositional ages of paleowetland sediments, Las Vegas Valley, Nevada. *Quaternary Geochronology*, 48, 80–90. https://doi.org/10.1016/j.quageo.2018.07.006

Hardt, J. & Böse, M. (2016) The timing of the Weichselian Pomeranian ice marginal position south of the Baltic Sea: A critical review of morphological and geochronological results. *Quaternary International*, 478, 51–58. https://doi.org/10.1016/j.quaint.2016.07.044

Heine, K., Reuther, A.U., Thieke, H.U., Schulz, R., Schlaak, N. & Kubik, P.W. (2009) Timing of Weichselian ice marginal positions in Brandenburg (northeastern Germany) using cosmogenic in situ ^{10}Be. *Zeitschrift für Geomorphologie*, 53(4), 433–454. https://doi.org/10.1127/0372-8854/2009/0053-0433

Hesp, P.A., Dillenburg, S.R., Barboza, E.G., Tomazelli, L.J., Ayup-Zouain, R. N., Esteves, L.S. et al. (2005) Beach ridges, foredunes or transgressive dunefields? Definitions and an examination of the Torres to Tramandaí barrier system, Southern Brazil. *Anais da Academia Brasileira de Ciências*, 77(3), 493–508. https://doi.org/10.1590/S0001-37652005000300010

Johnston, J.W., Thompson, T.A. & Baedke, S.J. (2007) Systematic pattern of beach-ridge development and preservation: Conceptual model and evidence from ground penetrating radar. *Geological Society of America Special Papers*, 432, 47–58. https://doi.org/10.1130/2007.2432(04)

Kaiser, K., Küster, M., Fülling, A., Theuerkauf, M., Dietze, E., Graventein, H. et al. (2014) Littoral landforms and pedosedimentary sequences indicating late Holocene lake-level changes in northern central Europe – a case study from northeastern Germany. *Geomorphology*, 216, 58–78. https://doi.org/10.1016/j.geomorph.2014.03.025

Kaiser, K., Schneider, T., Küster, M., Dietze, E., Fülling, A., Heinrich, S. et al. (2020) Palaeosols and their cover sediments of a glacial landscape in northern central Europe: Spatial distribution, pedostratigraphy and evidence on landscape evolution. *Catena*, 193, 104647. https://doi.org/10.1016/j.catena.2020.104647

Konze, M. (2017) *Bergung und Dokumentation von Teilen des Bodendenkmals "Schloss Schwerin" (Fpl. 17) im Rahmen des Projektes "Schloss Schwerin, Ver- und Entsorgungsleitungen im Innenhof" (3544–4098-HS)*. Schwerin: Ladesamt für Kultur und Denkmalpflege Mecklenburg-Vorpommern.

Krienke, H.-D. & Obst, K. (2011) Raben Steinfeld und die Eiszeit – Landschaftsentwicklung und geologische Sehenswürdigkeiten südöstlich von Schwerin. *Brandenburgische Geowissenschaftliche Beiträge*, 18(1/2), 107–123.

Küster, M. (2013). Holozäne Landschaftsentwicklung der Mecklenburgischen Seenplatte: Relief- und Bodengenese, hydrologische Entwicklung sowie Siedlungs- und Landnutzungsgeschichte in Nordostdeutschland. Dissertation. Greifswald.

Lampe, M. & Lampe, R. (2018) Evolution of a large Baltic beach ridge plain (Neudarss, NE Germany): A continuous record of sea-level and wind-field variation since the Homeric Minimum. *Earth Surface Processes and Landforms*, 43(15), 3042–3056. https://doi.org/10.1002/esp.4468

Lampe, R., Lorenz, S., Janke, W., Meyer, H., Küster, M., Hübener, T. & Schwarz, A. (2009) *Zur Landschafts- und Gewässergeschichte der Müritz: Umweltgeschichtlich orientierte Bohrungen 2004–2006 zur Rekonstruktion der nacheiszeitlichen Entwicklung*. Geozon Science Media: Greifswald.

Lorenz, S. (2007) Die spätpleistozäne und holozäne Gewässernetzentwicklung im Bereich der Pommerschen Haupteisrandlage Mecklenburgs. PhD thesis, Greifswald.

Muñoz-Salinas, E., Bishop, P., Sanderson, D. & Kinnaird, T. (2014) Using OSL to assess hypotheses related to the impacts of land use change with the early nineteenth century arrival of Europeans in south-eastern Australia: An exploratory case study from Grabben Gullen Creek, New South Wales. *Earth Surface Processes and Landforms*, 39(12), 1576–1586. https://doi.org/10.1002/esp.3542

Muñoz-Salinas, E., Bishop, P., Sanderson, D.C.W. & Zamorano, J.-J. (2011) Interpreting luminescence data from a portable OSL reader: Three case studies in fluvial settings. *Earth Surface Processes and Landforms*, 36(5), 651–660. https://doi.org/10.1002/esp.2084

Muñoz-Salinas, E., Bishop, P., Zamorano, J.-J. & Sanderson, D. (2012) Sedimentological processes in lahars: Insights from optically stimulated luminescence analysis. *Geomorphology*, 136(1), 106–113. https://doi.org/10.1016/j.geomorph.2011.06.024

Munyikwa, K., Kinnaird, T.C. & Sanderson, D.C. (2021) The potential of portable luminescence readers in geomorphological investigations: A review. *Earth Surface Processes and Landforms*, 46(1), 131–150. https://doi.org/10.1002/esp.4975

Murray, A.S. & Olley, J.M. (2002) Precision and accuracy in the optical stimulated luminescence dating of sedimentary quartz: A review. *Geochronometria*, 21, 1–16.

Murray, A.S. & Wintle, A.G. (2000) Luminescence dating of quartz using an improved single-aliquot regenerative-dose protocol. *Radiation Measurements*, 32(1), 57–73. https://doi.org/10.1016/S1350-4487(99)00253-X

Murray, A.S. & Wintle, A.G. (2003) The single aliquot regenerative dose protocol: Potential for improvements in reliability. *Radiation Measurements*, 37(4–5), 377–381. https://doi.org/10.1016/S1350-4487(03)00053-2

Nixdorf, B., Hemm, M., Hoffmann, A. & Richter, P. (2004) *Dokumentation von Zustand und Entwicklung der wichtigsten Seen Deutschlands: Teil 2 - Mecklenburg-Vorpommern*. Cottbus: Brandenburgische Technische Universität.

Nott, J., Forsyth, A., Rhodes, E. & O'Grady, D. (2015) The origin of centennial- to millennial-scale chronological gaps in storm emplaced beach ridge plains. *Marine Geology*, 367, 83–93. https://doi.org/10.1016/j.margeo.2015.05.011

Nott, J., Smithers, S., Walsh, K. & Rhodes, E. (2009) Sand beach ridges record 6000 year history of extreme tropical cyclone activity in northeastern Australia. *Quaternary Science Reviews*, 28(15–16), 1511–1520. https://doi.org/10.1016/j.quascirev.2009.02.014

Otvos, E.G. (2000) Beach ridges – definitions and significance. *Geomorphology*, 32(1–2), 83–108. https://doi.org/10.1016/S0169-555X(99)00075-6

Petty, W.H., Delcourt, P.A. & Delcourt, H.R. (1996) Holocene lake-level fluctuations and beach-ridge development along the northern shore of Lake Michigan, USA. *Journal of Paleolimnology*, 15(2), 147–169. https://doi.org/10.1007/BF00196778

Portenga, E.W. & Bishop, P. (2016) Confirming geomorphological interpretations based on portable OSL reader data. *Earth Surface Processes and Landforms*, 41(3), 427–432. https://doi.org/10.1002/esp.3834

Preusser, F., Degering, D., Fuchs, M., Hilgers, A., Kadereit, A., Klasen, N. et al. (2008) Luminescence dating: Basics, methods and applications. *E&G Quaternary Science Journal*, 57(1), 95–149. https://doi.org/10.3285/eg.57.1-2.5

Reimer, P.J., Austin, W.E.N., Bard, E., Bayliss, A., Blackwell, P.G., Bronk Ramsey, C. et al. (2020) The IntCal20 Northern Hemisphere Radiocarbon Age Calibration Curve (0–55 cal kBP). *Radiocarbon*, 62(4), 1–33. https://doi.org/10.1017/RDC.2020.41

Rhodes, E.J. (2011) Optically stimulated luminescence dating of sediments over the past 200,000 years. *Annual Review of Earth and Planetary Sciences*, 39(1), 461–488. https://doi.org/10.1146/annurev-earth-040610-133425

Rinterknecht, V., Börner, A., Bourlès, D. & Braucher, R. (2014) Cosmogenic ^{10}Be dating of ice sheet marginal belts in Mecklenburg-Vorpommern, Western Pomerania (northeast Germany). *Quaternary Geochronology*, 19, 42–51. https://doi.org/10.1016/j.quageo.2013.05.003

Sanderson, D.C.W. & Murphy, S. (2010) Using simple portable OSL measurements and laboratory characterisation to help understand complex and heterogeneous sediment sequences for luminescence dating. *Quaternary Geochronology*, 5(2–3), 299–305. https://doi.org/10.1016/j.quageo.2009.02.001

Scheffers, A., Engel, M., Scheffers, S., Squire, P. & Kelletat, D. (2012) Beach ridge systems – archives for Holocene coastal events? *Progress in Physical Geography: Earth and Environment*, 36(1), 5–37. https://doi.org/10.1177/0309133311419549

Stang, D.M., Rhodes, E.J. & Heimsath, A.M. (2012) Assessing soil mixing processes and rates using a portable OSL-IRSL reader: Preliminary determinations. *Quaternary Geochronology*, 10, 314–319. https://doi.org/10.1016/j.quageo.2012.04.021

Stone, A., Bateman, M.D., Burrough, S.L., Garzanti, E., Limonta, M., Radeff, G. & Telfer, M.W. (2019) Using a portable luminescence reader for rapid age assessment of aeolian sediments for reconstructing dunefield landscape evolution in southern Africa. *Quaternary Geochronology*, 49, 57–64. https://doi.org/10.1016/j.quageo.2018.03.002

Stone, A., Bateman, M.D. & Thomas, D. (2015) Rapid age assessment in the Namib Sand Sea using a portable luminescence reader. *Quaternary Geochronology*, 30, 134–140. https://doi.org/10.1016/j.quageo.2015.02.002

Storms, J.E.A. & Kroonenberg, S.B. (2007) The impact of rapid sea level changes on recent Azerbaijan beach ridges. *Journal of Coastal Research*, 232, 521–527. https://doi.org/10.2112/05-0622.1

Stuiver, M., Reimer, P.J. & Reimer, R.W. (2020) CALIB 8.20 [WWW program]. http://calib.org.

Tamura, T. (2012) Beach ridges and prograded beach deposits as palaeoenvironment records. *Earth-Science Reviews*, 114(3–4), 279–297. https://doi.org/10.1016/j.earscirev.2012.06.004

Tamura, T., Oliver, T.S.N., Cunningham, A.C. & Woodroffe, C.D. (2019) Recurrence of extreme coastal erosion in SE Australia beyond historical timescales inferred from beach ridge morphostratigraphy. *Geophysical Research Letters*, 46(9), 4705–4714. https://doi.org/10.1029/2019GL083061

Tanner, W.F. (1995) Origin of beach ridges and swales. *Marine Geology*, 129, 149–161. https://doi.org/10.1016/0025-3227(95)00109-3

Thompson, T.A. (1992) Beach-ridge development and lake-level variation in southern Lake Michigan. *Sedimentary Geology*, 80(3–4), 305–318. https://doi.org/10.1016/0037-0738(92)90048-V

Thompson, T.A. & Baedke, S.J. (1995) Beach-ridge development in Lake Michigan: Shoreline behavior in response to quasi-periodic lake-level events. *Marine Geology*, 129(1–2), 163–174. https://doi.org/10.1016/0025-3227(95)00110-7

Thompson, T.A. & Baedke, S.J. (1997) Strand-plain evidence for late Holocene lake-level variations in Lake Michigan. *Geological Society of America Bulletin*, 109(6), 666–682. https://doi.org/10.1130/0016-7606(1997)109<0666:SPEFLH>2.3.CO;2

von Carmer, C.F. (2006) Gewässerkulturlandschaften – Die historische Dimension kleiner Fließgewässer am Beispiel des Wallensteingrabens. *Wasserwirtschaft*, 7–8, 28–32. https://doi.org/10.1007/BF03241337

SUPPORTING INFORMATION

Additional supporting information may be found in the online version of the article at the publisher's website.

How to cite this article: Adolph, M.-L., Lampe, R., Lorenz, S. & Haberzettl, T. (2022) Characterization of (paleo)lacustrine landforms using sedimentological and portable OSL investigations at Schweriner See, north-eastern Germany. *Earth Surface Processes and Landforms*, 47(2), 422–435. Available from: https://doi.org/10.1002/esp.5258